Heliyon 9 (2023) e16269

Contents lists available at ScienceDirect

Heliyon

journal homepage: www.cell.com/heliyon

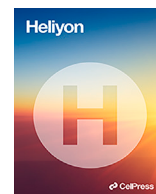

Research article

Bias and illumination-dependent room temperature negative differential conductance in Ni-doped ZnO/p-Si Schottky photodiodes for quantum optics applications

Richard O. Ocaya [a,*], Yusuf Orman [b], Abdullah G. Al-Sehemi [c,d,e], Aysegul Dere [f], Ahmed A. Al-Ghamdi [g], Fahrettin Yakuphanoğlu [b]

[a] Department of Physics, University of the Free State, P. Bag X13, Phuthaditjhaba 9866, South Africa
[b] Department of Physics, Faculty of Science, Firat University, Elaziğ, Turkey
[c] Department of Chemistry, Faculty of Science, King Khalid University, Abha 61413, P.O. Box 9004, Saudi Arabia
[d] Research Center for Advanced Materials Science, King Khalid University, Abha 61413, P.O. Box 9004, Saudi Arabia
[e] Unit of Science and Technology, Faculty of Science, King Khalid University, Abha 61413, P.O. Box 9004, Saudi Arabia
[f] Vocational School of Technical Science, Department of Electric and Energy, Firat University, Elaziğ, Turkey
[g] Department of Physics, Faculty of Science, King Abdulaziz University, Jeddah 21589, Saudi Arabia

A R T I C L E I N F O

Keywords:
Negative differential conductivity
Series resistance compensation
Ni-doped ZnO
Illumination
Bias

A B S T R A C T

In this article, evidence for the existence of illumination and bias-dependent negative differential conductance (NDC) in Ni-doped Al/ZnO/p-Si Schottky diodes, and the possible mechanism for its origin, are presented. The atomic percentages of Ni doping were 0%, 3%, 5%, and 10%. NDC is observed between -1.5 V to -0.5 V in reverse bias under illumination, but only at certain doping levels and specific forward bias. Furthermore, the devices show excellent optoelectronic characteristics in the photoconductive and photovoltaic modes, with device open circuit voltages ranging from 0.03 V to 0.6 V under illumination.

1. Introduction

At present, ZnO remains the poster child for exciting metal oxides for new devices because of its optical and electrical properties. It holds this position for its low cost and high experimental accessibility, and the potential for optimization through stable, co-doping with other elements [1]. ZnO has a remarkable propensity to host many elements in the periodic table; there are growing reports of its beneficial alloys with elements of comparable ionic radii and suitable electronic configuration, with the list now including alkali/earth metals, lanthanides, actinides, and non-metals [2]. Some recent examples are Mg, Gd, Mn, Cu, Ti, Co, Cd, Cr, Fe, V, etc, for application in photocatalysis, electronics and optoelectronics, spintronics, magnetic sensors, medicine, etc [3,4,2]. Unalloyed ZnO is theoretically limited by a phenomenon that increases the prevalence of interface states with a p-Si substrate, with a net lowering of the conduction band and enhancement of carrier recombination in the trap states. This encourages recombination within the junction, with fewer carriers recombining at the electrodes. This increases the mismatch between ZnO and p-Si which, in a solar cell, manifests externally as a lowered open-circuit voltage (V_{oc}) [3]. In photoconductive devices, it is seen as a lowered device current. It was proposed to co-dope ZnO with elements that tune its band gap by raising its conduction band and reducing recombinations.

* Corresponding author.
E-mail address: ocayaro@ufs.ac.za (R.O. Ocaya).

https://doi.org/10.1016/j.heliyon.2023.e16269
Received 18 February 2023; Received in revised form 5 May 2023; Accepted 11 May 2023

Available online 18 May 2023
2405-8440/© 2023 The Author(s). Published by Elsevier Ltd. This is an open access article under the CC BY-NC-ND license (http://creativecommons.org/licenses/by-nc-nd/4.0/).

Such efforts are the main drivers of the current research in an attempt to gain a fuller understanding of the underlying processes involved in ZnO charge transport, particularly in its nanostructured composite films. This is done by evaluating the doped bandgap, the surface potentials and substrate compatibilities, and the transparencies of the alloyed films, using a wide spectrum of techniques. For semiconductor device applications, a persistent challenge has been to devise methods that achieve p-ZnO consistently, which is generally harder than for n-ZnO [5,1]. Other transparent conductive metal oxides, particularly indium-tin (ITO), though potent, are today less preferred for large-area devices like heterojunction solar cells (HJSC) because of the cost of rare earth elements, or their peculiar processing requirements [6]. In the last decade, ZnO-based HJSCs have been demonstrated with photovoltaic power conversion efficiencies (PCE) $>15\%$ [7]. ZnO has also found widespread application in photoconductive, gas, and other sensors [8–10].

In this article, we present evidence of room temperature (300 K) NDC in suitably Ni-doped ZnO metal–semiconductor–metal (MSM) Schottky photodiodes configured in the Al/(Ni:ZnO)/p-Si/Al structure. The electronegativity and ionic radius (r) of Ni ($r = 0.69$ Å) imply an affinity and good substitutional compatibility with Zn ($r = 0.74$ Å) with minimal distortion of the host structure [11]. Prior studies have shown that Ni doping maintains ZnO film transparency [12] while enhancing the electrical conductivity through two extra electrons. However, the trade-off is a reduction in the band gap e.g. to as low as ∼3.15 (6% Ni) from ∼3.37 eV (undoped) [13,14]. By the foregoing arguments, the distribution of interface states is also enhanced with new carrier valleys introduced in the band gap. Measurements have shown that there is a redshift, indicating enhanced absorption of Ni:ZnO in the visible spectral regions, up from the ultraviolet region. Hussain et al. [7] were the first to report low-temperature NDC in Ni/Ge transferred electron Schottky diodes. The NDC regions in the presented devices are dependent on the illumination and electric field applied to the detecting area of the devices. NDC regions have been reported in some new devices, with various explanations being given for the underlying mechanisms [15,16]. NDC in quantum-well devices is well studied, with increasing literature reports of the phenomenon in heterojunction and superlattice devices. Also, these structured devices have many possible causative factors for the NDC in both forward and reverse bias. In short, the underlying mechanisms are not yet fully understood. Explanations based on varied phenomena, such as capacitive blockade, Γ–X resonances, single-electron, intervalley electron transfers, quantum mechanical tunneling, and other effects, have been put forth [17–20]. Empirical and computational studies in varied contexts, e.g. Ma et al. [21], Haq et al. [22], Ho et al. [18], etc, suggest that doping creates valleys/subbands such that applied field causes differential carrier mobilities, in line with the RWH mechanism in forward bias [23], or quantum mechanical tunneling at low reverse biases. The degree of doping must be kept below a level that degenerates the band gap into a near-metallic character. In the RWH mechanism, the application of a higher field causes the transfer of some electrons to a higher valley/subband where their effective mass is higher thus reducing their mobility and the net current. The effect resolves once the applied field exceeds the threshold, where the electrons reside fully in the upper valley/subband. The current density then continues to increase with the applied field. Haq et al. [22] calculated the density of states of ZnO doped with up to 25% Ni. They found that the interplay of the electron states in Zn, Ni, and O is highly dependent on the applied energy. At lower energies, the peaks in the DOS arise from the Zn^{3d} and O^{2p} electron states. At higher energies, it is mainly due to the Ni^{3d} and O^{2p} electron states. The change of the mobilities due to the field control of the electron population could account for the differential conductance. A further interesting aspect of Ni doping is the potential impact of its ferromagnetism owing to the two unpaired electrons, due to its likely impact on the localized carrier mobility near Ni sites. Whether these two electrons are responsible through their magnetic moment to the NDC is arguable. Still, experimentation with a dopant with a higher magnetic moment, such as Fe (4 unpaired electrons), would add some clarity. For the presented devices, additional electrical and impedance spectroscopic measurements on the fabricated devices were done. The phenomenon may have escaped deeper scrutiny over the last few decades owing to limiting post-experiment I-V analysis methods, such as the popular Cheung-Cheung method [24]. These methods linearize the series resistance over the empirical bias region and, therefore, inadvertently smooth out potential NDC anomalies on the bias range. A recently devised method [25] proved rigorously that the true series resistance (R_s) in the thermionic emission equation is the instantaneous dynamic resistance. R_s compensation then allows focusing on the peculiarities of the I-V results. The results show that in reverse bias, all levels of Ni doping yield NDC regions under illumination, but are selective to doping level in forward bias. The presence of Ni below 10% does not significantly enhance the photovoltaic characteristics, although the open-circuit voltage approaches the theoretical 0.6 V at 10% Ni.

2. Experimental

The Nickel-doped ZnO materials were synthesized as follows according to the outlines described by Ayachi et al., and Al-Ariki et al. [12,26]. Firstly, 0.5 M of zinc acetate dihydrate was dissolved in 2-methoxyethanol for 1 hour at 60 °C while stirring. The various contents of Nickel-doped ZnO solutions were prepared with atomic ratios of 1%, 3%, 5%, and 10%. The prepared solutions were stirred for 10 minutes, and then monoethanolamine was added to these solutions. They were then stirred for 1 hour at 60 °C. To prepare Ni-doped ZnO/p-Si diodes, Ni-doped ZnO films were coated on p-Si wafers with ohmic contacts, and the films were annealed at 450 °C for 1 hour under a nitrogen atmosphere. The thicknesses of 1%, 3%, 5%, and 10% Ni doped films were measured using a FYTRONIX film thickness analyzer [27]. The measured values were found to be 122.1 ±0.13 nm for the 1% Ni doped film, 132.1 ±0.11 nm for the 3% Ni doped film, 128.2±0.15 nm for the 5% Ni doped film, and 145.3±0.13 nm for the 10% Ni doped film. Top Al contacts with a 2 mm diameter were then prepared on the Ni-doped ZnO films using a thermal evaporation system. Current-voltage, capacitance-voltage, and photo transient measurements were performed using an FYTRONIX Semiconductor characterization system, which includes an AAA class solar simulator, I-V analyzer, and C-V analyzer [28,29,27].

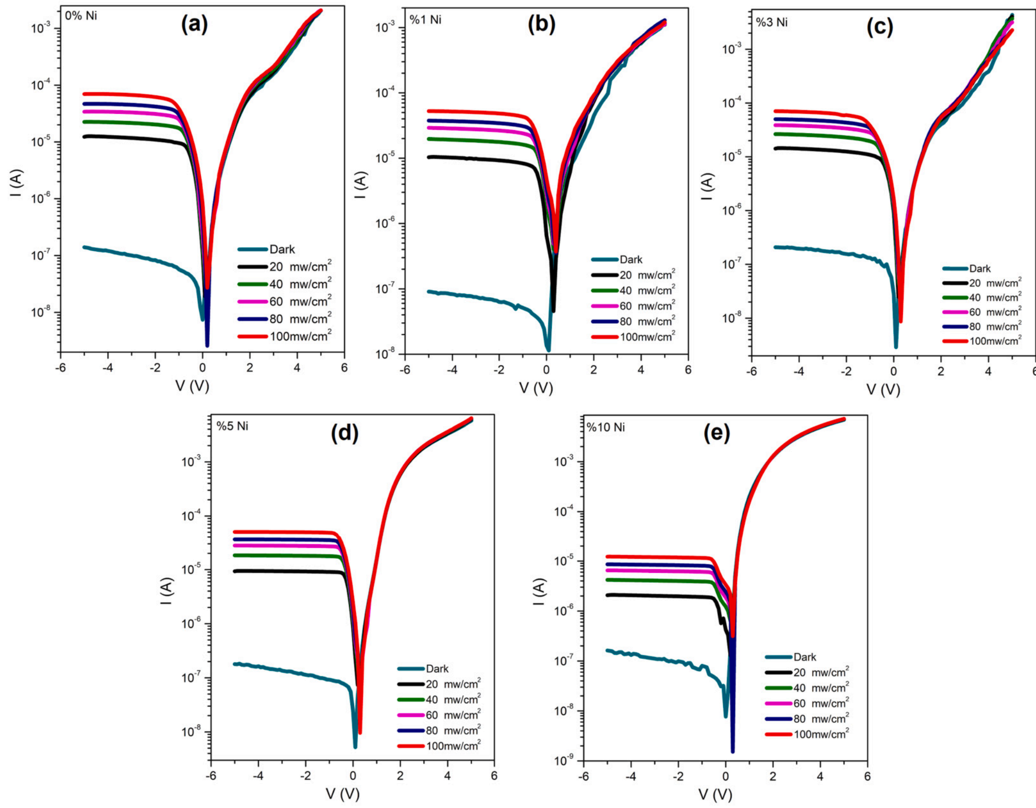

Fig. 1. The measured I-V characteristics of the diodes with different Ni doping. The illumination intensity is varied from 0 to 100 mW/cm^2. The Ni concentration is 0, 1, 3, 5, and 10% in (a), (b), (c), (d), and (e), respectively.

3. Results and discussion

3.1. Current-voltage characterization

The current through a Schottky diode in the thermionic emission theory is given by [30,31]

$$y = \frac{e^{[-b\phi(x)+cz]}(1-e^{-bz})}{s}, \tag{1}$$

where $y = I$, $z = (V\text{-}IR_s)$ is the R_s compensated bias, $b = q/kT$, $c = b/n$, $r = R_s$, and $s = 1/AA^*T^2$. We assume that the barrier height is constant s.t. $\phi = \Phi_0$. Then Eq. (1) becomes

$$y = e^{cz}(1-e^{-bz})/p. \tag{2}$$

At the low biases typical in such Schottky diodes Eq. (2) can be approximated by $\ln y = (cz - \ln p)$, where $s = p\exp(-b\Phi_0)$. A semilog plot of the R_s compensated I-V characteristics is linear, with the intercept $\alpha = \ln p^{-1}$, and ideality factor $n = q/ckT$. This gives the well-known result [32]

$$\Phi_0 = \frac{kT}{q}\ln\left(\frac{AA^*T^2}{I_0}\right), \tag{3}$$

where $I_0 = 1/p$ is the zero bias thermionic current. At typical measurement conditions Eq. (3) implies that Φ_0 approximately linear in the temperature since $kT \gg \ln(pAA^*T^2)$ [33]. The non-ionized acceptor density then [34,35]

$$N_a \approx N_v \exp\left\{\frac{q(V_p - n\Phi_0)}{nkT}\right\}, \tag{4}$$

where $V_p = E_f\text{-}E_v$, where E_f is the Fermi level, and E_v is the maximum valence energy in the neutral part of p-type Si. The valence band hole density of states N_v in p-Si is circa $1.04\times10^{19}/\text{cm}^3$. Fig. 1 (a)-(e) shows the measured I-V characteristics of the diodes for different Ni content.

Fig. 2 (a) shows the averaged plots using the measurements for 0% Ni for illustration. Fig. 2 (b) shows the two regions L1 and L2 where the parameters were determined. The least-squares fitting of each low and high bias region produced a slope, intercept, and standard error pair for the characteristic.

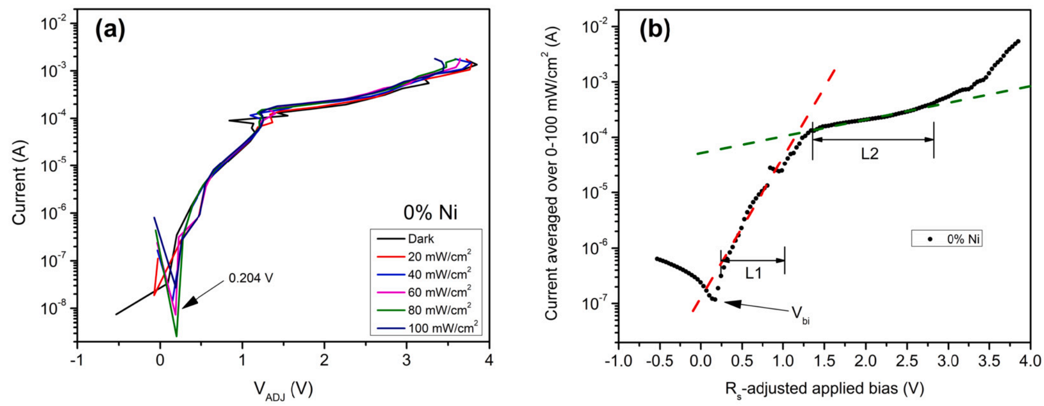

Fig. 2. In (a), the typical Method 1 plot of forward bias current averaged over intensity, using the example of 0% Ni content in ZnO. In (b), averaging of the curves in (a), see text. The dotted lines are the least-squares fits of the low and high bias regions L1 and L2, respectively. The built-in potential is V_{bi}.

Fig. 3. Color map representation of $\ln R_s(\mathrm{k})$ versus applied bias, %Ni content, and illumination. The illumination intensities are 0, 20, 60 and 100 mW/cm^2 in (a), (b), (c), and (d), respectively.

The plots suggest that R_s is strongly affected by bias but not illumination. Fig. 3 is the color map of the calculated series resistance under various conditions of bias, Ni content, and illumination. The obtained R_s compensated I-V characteristics in the forward bias under dark to 100 mW/cm^2 at a given Ni-content in ZnO were visually similar and were, therefore, averaged to a single trace before applying the foregoing equations. Fig. 4 (a) is a surface plot of the R_s-compensated forward bias I-V characteristics over varying Ni

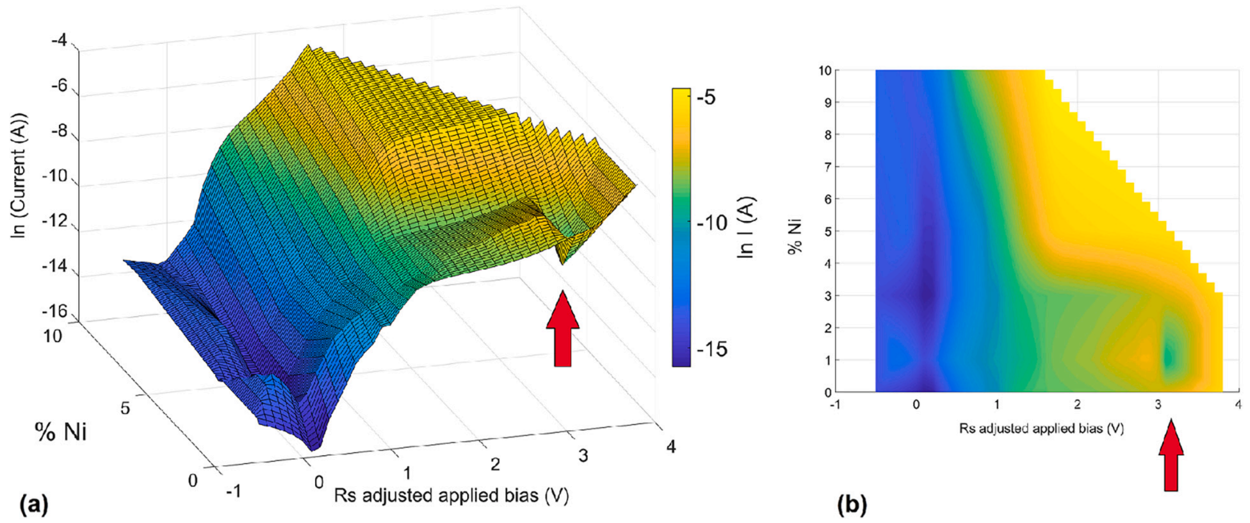

Fig. 4. In (a), the surface plot of the R_s-compensated forward bias I-V characteristics for varying % Ni content with its color map, (b). In each plot, the arrow shows a region of negative resistance.

Table 1
Method 1 results for the diodes constructed with different Ni %, excluding R_s, since Method 1 predicts that R_s is bias-dependent.

%Ni	Region	$\Phi_0 \pm 0.004$ (eV)	n	Io (μA)
0	L1	0.637	9.0	0.438
	L2	0.533	36.1	24.7
1	L1	0.632	7.1	0.521
	L2	0.561	22.3	8.48
3	L1	0.637	9.0	0.438
	L2	0.533	36.1	24.7
5	L1	0.664	6.6	0.155
	L2	0.271	5.9	1346
10	L1	0.651	3.5	0.254
	L2	0.538	11	0.206

content. Fig. 4 (b) is the contour map of the same plot which facilitates recognition of the negative resistance region, as indicated by the arrow.

Method 2 is the Cheung and Cheung method [24], with the functions (Tables 1 and 2):

$$\begin{aligned}\frac{dV}{d\ln I} &= R_s I + \frac{nkT}{q},\\ H(I) &= R_s I + n\Phi_b,\\ &= \left[V - \frac{nkT}{q}\ln\left(\frac{I}{AA^*T^2}\right)\right].\end{aligned} \tag{5}$$

ZnO/p-Si diodes in various configurations have the following typical parameter values: $\Phi_0 = 0.7$ eV, $V_{bi} = 0.66$ V, and N_A between 10^{15} and 10^{16} /cm^3 for the average acceptor density [36–40]. The Method 1 results in Table 3 have the closest match to those of Ocak [36].

3.2. Impedance characteristics

A metal oxide semiconductor (MOS) C-V characteristic normally shows the regions associated with charge accumulation, charge depletion, and charge inversion. At temperature T, the device capacitance at applied bias (V) is [41,42,31,30,43]

$$\frac{1}{C^2} = -\frac{2}{q\varepsilon_s A^2 N_A}\left(V - V_{bi} + \frac{kT}{q}\right). \tag{6}$$

The net dielectric permittivity for p-Si is $\varepsilon_s = 11.8\varepsilon_0$, where $\varepsilon_0 = 0.08854$ pF/cm. The area of the device is A. The plot of $1/C^2$ versus V using Eq. (6) at a given temperature gives a gradient that is used to estimate N_A, and an intercept that is used to estimate V_{bi}. Fig. 5 are the 3-D plots of the C-V-f variations at different Ni%. Fig. 6 are the corresponding colors maps.

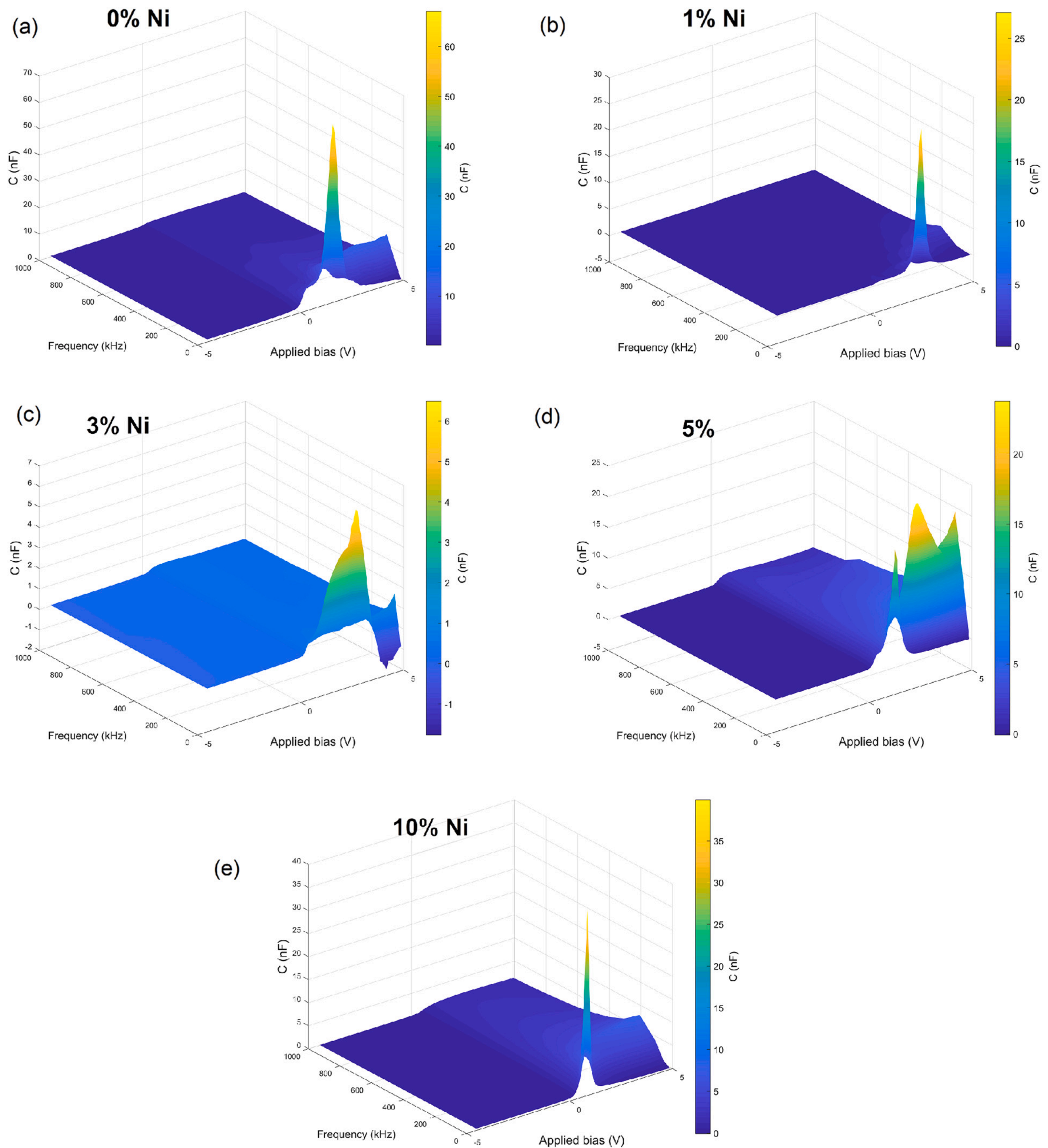

Fig. 5. Variations of capacitance with applied bias and frequency with %Ni content. The Ni concentration is 0, 1, 3, 5 and 10% in (a), (b), (c), (d) and (e), respectively.

Table 3 summarizes the results of V_{bi}, and N_A using Method 1 and the C-V method. N_a corresponds to a 300 K p-Si resistivity of 9–15 Ωcm. This result matches the square resistance of the substrates used for the diodes. C-V impedance measurements were made at 10 kHz, with V_{bi} reported increasing to 0.5 V with frequency. The barrier height is determined using Eq. (4).

The nonionized acceptor density was calculated from the C-V method over all frequencies.

3.3. Electrical photo-responses

The equivalent circuit in Fig. 7 was used to determine the R_s-compensated photoconductive and photovoltaic responses shown in Fig. 9. The plots show that NDC regions are observed in the 0, 3, and 5% doped devices in forward bias. In reverse bias, for biases

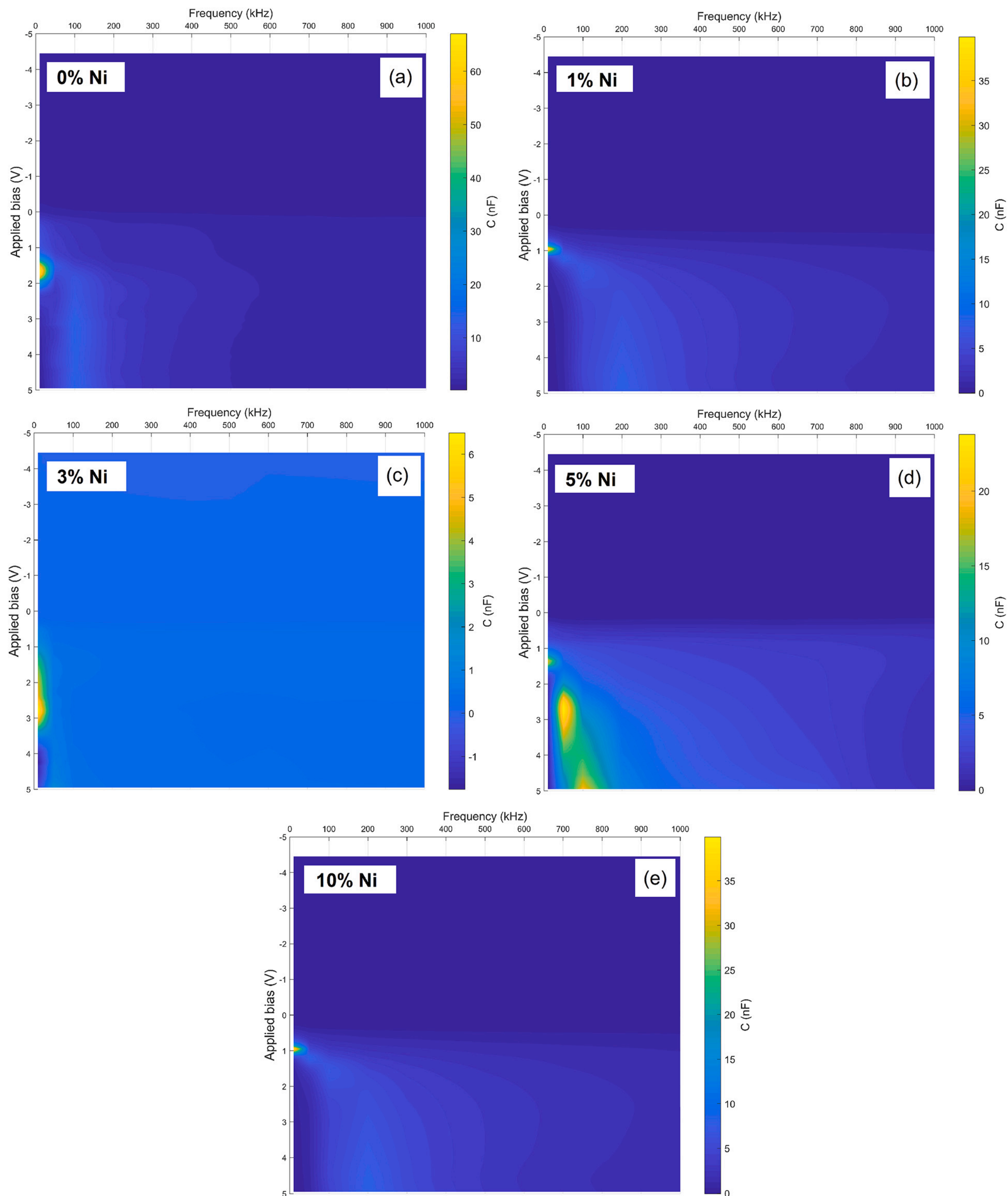

Fig. 6. Variations of capacitance with applied bias and frequency for different %Ni content. The Ni concentration is 0, 1, 3, 5 and 10% in (a), (b), (c), (d) and (e), respectively.

between -1.5 V and 0 V, all devices exhibit NDC. In the reverse bias mode, there is no evidence of NDC behavior in the characteristics. Thus, both bias and illumination contribute to the onset of the observed NDC. Most NDCs in heterojunction devices in the literature are reported in the reverse bias region.

Table 2
Method 2 results for the diodes constructed with different Ni %. Method 2 assumes that R_s is constant in the bias region of 0.5 V to 2.5 V, where the functions of Eq. (5) are linear.

%Ni	Parameter	0	20	40	60	80	100
		(mW/cm^2)					
0	n	7.2	9.1	6.9	8.5	6.9	7.4
	Φ_0 (eV)	0.643	0.508	0.665	0.540	0.659	0.615
	Rs (k)	10.3	8.6	8.1	6.6	7.2	6.9
1	n	18.9	14.9	19.2	15.4	20.1	22.2
	Φ_0 (eV)	0.284	0.348	0.266	0.333	0.260	0.229
	Rs (k)	2.3	2.6	2.3	2.8	2.1	2.1
3	n	5.6	6.6	6.7	7.3	5.9	7.1
	Φ_0 (eV)	0.816	0.697	0.692	0.631	0.783	0.656
	Rs (k)	19.4	14.5	13.1	12.1	12.3	11.4
5	n	6.5	6.1	9.1	12.1	6.7	7.0
	Φ_0 (eV)	0.698	0.747	0.498	0.376	0.674	0.650
	Rs (k)	0.62	0.60	0.56	0.53	0.57	0.56
10	n	10.1	4.6	5.0	5.5	6.0	5.5
	Φ_0 (eV)	0.396	0.841	0.782	0.714	0.657	0.701
	Rs (k)	0.62	0.72	0.72	0.70	0.67	0.65

Table 3
Method 1 calculated built-in voltage, V_{bi}, and the C-V method-calculated non-ionized acceptor density, N_A, at 10 kHz.

	Method 1	C-V method		
% Ni	V_{bi} (V)	V_{bi} (V)	Φ_0 (eV)	$N_a(10^{14})$ (/cm^3)
0	0.204	0.116	0.355	10.0±3.0
1	0.197	0.415	0.651	11.0±6.0
3	0.192	0.354	0.594	9.6±1.2
5	0.173	0.220	0.454	12.4±3.4
10	0.287	0.171	0.412	9.2±0.8

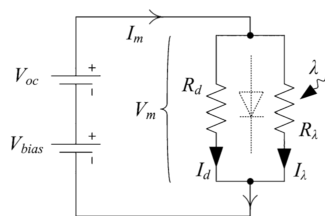

Fig. 7. The basic reverse and forward bias photo-response measurement circuit. In reverse bias, $V_{oc} = 0$. To measure the photovoltaic V_{oc}, set $V_{bias} = 0$.

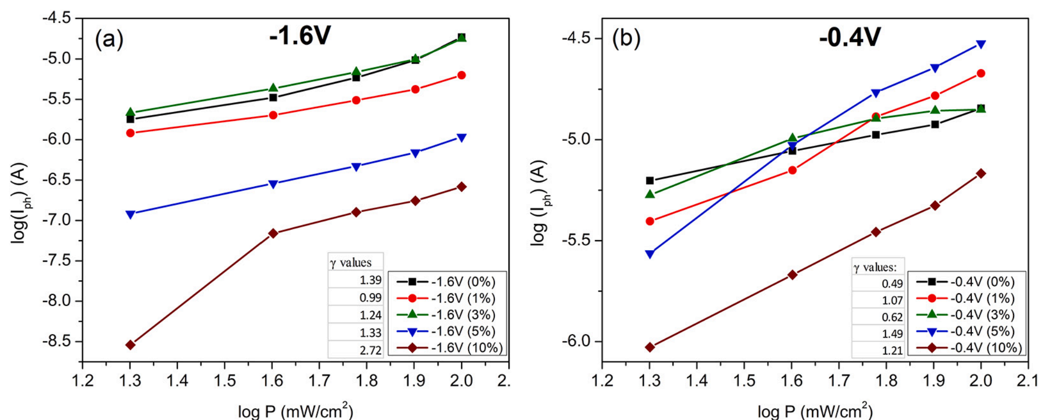

Fig. 8. Plots showing a power-law dependence of device photocurrents on illumination and %Ni content at arbitrary biases of, in (a) -1.6 V and, in (b) -0.4 V. Doping at 1%Ni gave both bias regions a linear ($\gamma = 1$) photoconductive sensing behavior.

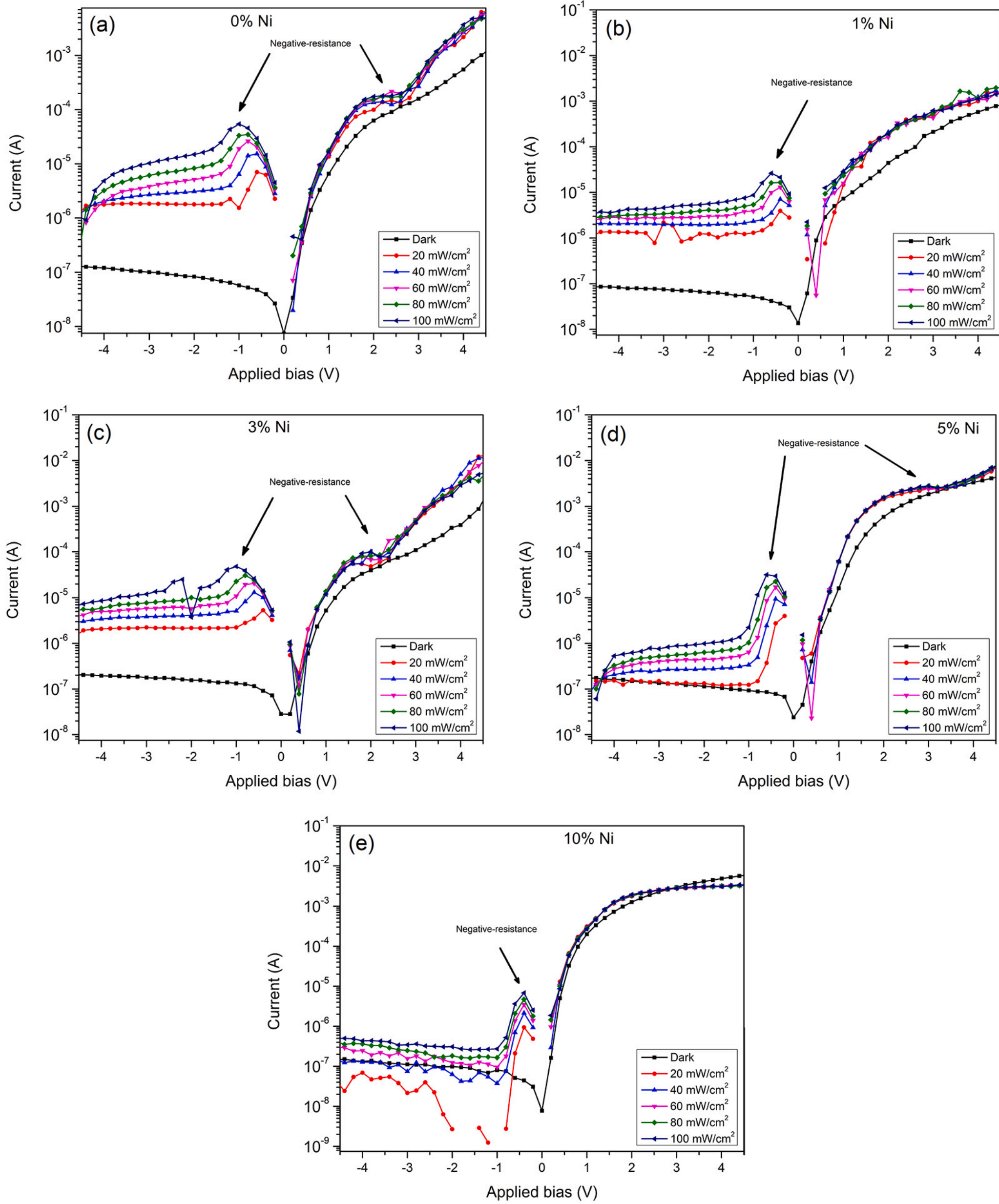

Fig. 9. R_s-corrected photo-conductive and voltaic currents, I_{ph}, for various % Ni content in fabricated diodes. The Ni concentration is 0, 1, 3, 5 and 10% in (a), (b), (c), (d) and (e), respectively. NDC regions are seen for all Ni doping levels at various reverse biases, but only at some doping levels in the forward bias.

In general, the short-circuit photocurrent is

$$I_\lambda = \frac{V_m}{R_s} - I_d, \tag{7}$$

where the total bias is $V_m = (V_{oc} + V_{bias})$, R_s is the parallel combination of R_λ and the dark resistance R_d, and I_d is the dark current. Both R_s and R_d are determined using Method 1.

3.3.1. Photoconductive response

The photoconductance power law [44,45]

$$I_\lambda = \alpha P^\gamma. \tag{8}$$

The index γ has been used to interpret the prevalent recombination mechanisms in the diode [44,46–48]. The plots in Fig. 8 obey the power law at arbitrary biases e.g. -1.6 V and -0.4 V. There is a strong bias dependence on γ, with lower reverse bias magnitudes

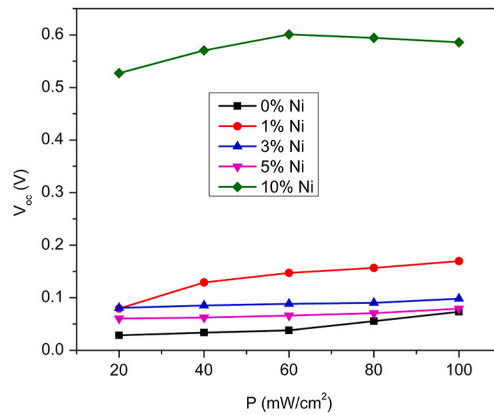

Fig. 10. R_s-corrected open-circuit voltages, V_{oc}, for various %Ni content in the fabricated diodes.

Fig. 11. Transient current responses of the diodes under 100 mW/cm^2 illumination and Ni concentrations of 0, 1, 3, 5 and 10% in (a), (b), (c), (d) and (e), respectively.

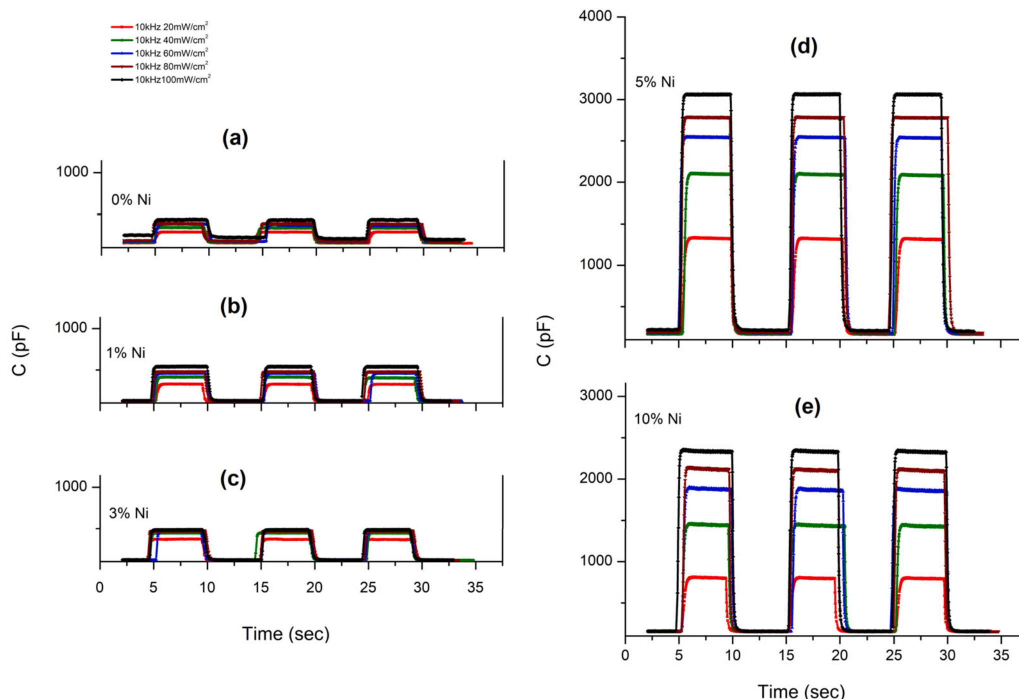

Fig. 12. Photo-capacitance responses of the diodes to 10 kHz, 50% duty-cycle illumination for varying Ni concentrations of 0, 1, 3, 5 and 10% in (a), (b), (c), (d) and (e), respectively.

generally favoring monomolecular recombination. At lower biases, however, increased doping favors bimolecular recombination. Higher magnitudes of reverse bias favor bimolecular recombination [28,49].

The observed photoconductive responses of the devices are comparable to those of similar p-Si/ZnO based diodes [50].

3.3.2. Photovoltaic response

The diode open-circuit voltage, V_{oc}, is a photovoltaic parameter that was estimated by setting $V_{bias} = 0$ in Eq. (7). The photocurrent is then the Norton current. Fig. 10 shows the calculated V_{oc} under various illumination intensities. The amount of Ni in the devices influences V_{oc}, driving it towards the theoretical >0.6 V at 10% Ni doping [1].

The photovoltaic performance of the fabricated devices is comparable with those reported in the literature [51,37,38,52].

3.4. Transient photoresponse

Photocapacitance and photoconductance indicate the extent of photo-generated carrier trapping by over-capacitance [15]. Fig. 11 and Fig. 12 show, respectively, the transient current and photo-capacitance responses of the fabricated diodes. Both of these figures show that the photocurrent and photo capacitance of 0% Ni devices exhibit two different stages during the rising process: a fast-rising process and a slow-rising process as a result of absorbing light. The reason for the different rates of the fast and slow processes is the oxygen molecule adsorption process on the surface of the p-Si/ZnO device. The oxygen molecule adsorption process for the fast-rising process is higher than that for the slow-rising process. This adsorption process changes the charge separation of a p-Si/ZnO junction, and as a result, the fast and slow rising processes occur in the depletion layer of the device.

The photo capacitance characteristics of the fabricated devices are comparable to those reported in the literature [53].

4. Conclusions

We have presented evidence of room temperature (300 K) NDC in suitably Ni-doped ZnO metal-semiconductor-metal photodiodes in the Al/(Ni:ZnO)/p-Si/Al configuration. The Ridley–Watkins–Hilsum (RWH) mechanism is suggested to account for the negative differential conductance in the diodes. All the presented devices exhibit NDC at specific biases between -1.5 V and -0.5 V. In forward bias, NDC was seen only for diodes with a specific doping level [54]. NDCs were shown to be bias- and illumination-dependent. The occurrence of NDC in I-V characteristics may be more widespread than previously appreciated as a result of the limiting nature of the methods used to characterize the series resistance. The measured V_{oc} of the devices ranged from 0.03 V to 0.6 V. The atomic percentages of Ni doping were 0%, 3%, 5%, and 10%. Future studies are required to understand the origin and mechanisms of NDC in similar metal–semiconductor–metal (MSM) photodiodes.

CRediT authorship contribution statement

Richard O. Ocaya: Analyzed and interpreted the data; Wrote the paper. **Yusuf Orman:** Conceived and designed the experiments; Analyzed and interpreted the data; Wrote the paper. **Abdullah G. Al-Sehemi:** Analyzed and interpreted the data. **Aysegul Dere:** Performed the experiments. **Ahmed A. Al-Ghamdi, Fahrettin Yakuphanoğlu:** Contributed reagents, materials, analysis tools or data.

Declaration of competing interest

The authors declare that they have no known competing financial interests or personal relationships that could have appeared to influence the work reported in this paper.

Data availability

Data will be made available on request.

Acknowledgements

The Research Center for Advanced Materials Science, King Khalid University, Kingdom of Saudi Arabia, is gratefully acknowledged for supporting this 207 research by Grant no. RCAMS/KKU/p002-21. Also, the support of FIRAT University Scientific Research Projects Unit by the ADEP-22.01, FF.12.19, and FF.22.17 grants is humbly acknowledged.

References

[1] B. Hussain, Improvement in open circuit voltage of n-ZnO/p-Si solar cell by using amorphous-ZnO at the interface, Prog. Photovolt. 25 (11) (2017) 919–927, https://doi.org/10.1002/pip.2906.
[2] P. Singh, R. Kumar, R.K. Singh, Progress on transition metal-doped ZnO nanoparticles and its application, Ind. Eng. Chem. Res. 58 (37) (2019) 17130–17163, https://doi.org/10.1021/acs.iecr.9b01561.
[3] K. Knutsen, R. Schifano, E. Marstein, B. Svensson, A.Y. Kuznetsov, Prediction of high efficiency ZnMgO/Si solar cells suppressing carrier recombination by conduction band engineering, Phys. Status Solidi (a) 210 (3) (2013) 585–588, https://doi.org/10.1002/pssa.201228527.
[4] S. Baturay, Y.S. Ocak, D. Kaya, The effect of Gd doping on the electrical and photoelectrical properties of Gd: ZnO/p-Si heterojunctions, J. Alloys Compd. 645 (2015) 29–33, https://doi.org/10.1016/j.jallcom.2015.04.212.
[5] M. Manabeng, B.S. Mwankemwa, R.O. Ocaya, T.E. Motaung, T.D. Malevu, A review of the impact of zinc oxide nanostructure morphology on perovskite solar cell performance, Processes 10 (9) (2022) 1803, https://doi.org/10.3390/pr10091803.
[6] M.A. Green, The path to 25% silicon solar cell efficiency: history of silicon cell evolution, Prog. Photovolt. 17 (3) (2009) 183–189.
[7] B. Hussain, A. Ebong, I. Ferguson, Zinc oxide as an active n-layer and antireflection coating for silicon based heterojunction solar cell, Sol. Energy Mater. Sol. Cells 139 (2015) 95–100, https://doi.org/10.1016/j.solmat.2015.03.017.
[8] A.J. Gimenez, J. Yáñez-Limón, J.M. Seminario, ZnO-paper based photoconductive UV sensor, J. Phys. Chem. C 115 (1) (2011) 282–287, https://doi.org/10.1021/jp107812w.
[9] Y. Kang, F. Yu, L. Zhang, W. Wang, L. Chen, Y. Li, Review of ZnO-based nanomaterials in gas sensors, Solid State Ion. 360 (2021) 115544, https://doi.org/10.1016/j.ssi.2020.115544.
[10] P. Kałużyński, W. Mucha, G. Capizzi, G. Lo Sciuto, Chemiresistor gas sensors based on conductive copolymer and ZnO blend–prototype fabrication, experimental testing, and response prediction by artificial neural networks, J. Mater. Sci., Mater. Electron. 33 (35) (2022) 26368–26382, https://doi.org/10.1007/s10854-022-09318-y.
[11] M.Y. Ali, M. Khan, A.T. Karim, M.M. Rahman, M. Kamruzzaman, Effect of Ni doping on structure, morphology and opto-transport properties of spray pyrolised ZnO nano-fiber, Heliyon 6 (3) (2020) e03588, https://doi.org/10.1016/j.heliyon.2020.e03588.
[12] M. Ayachi, F. Ayad, A. Djelloul, L. Benharrat, S. Anas, Synthesis and characterization of Ni-doped ZnO thin films prepared by sol–gel spin-coating method, Semiconductors 55 (5) (2021) 482–490, https://doi.org/10.1134/S1063782621050043.
[13] J. Eppakayala, M.R. Mettu, V.R. Pendyala, J.R. Madireddy, Synthesis, structural and optical properties of Ni doped ZnO nanoparticle–a chemical approach, Mater. Today Proc. 26 (2020) 148–153, https://doi.org/10.1016/j.matpr.2019.08.099.
[14] P.G. Undre, S.D. Birajdar, R. Kathare, K. Jadhav, Enhancement of electrical resistivity in Nickel doped ZnO nanoparticles, Proc. Manuf. 20 (2018) 477–480, https://doi.org/10.1016/j.promfg.2018.02.070.
[15] D.-K. Lee, H. Ko, Y. Cho, Single Si submicron wire photodetector fabricated by simple wet etching process, Mater. Lett. 160 (2015) 562–565, https://doi.org/10.1016/j.matlet.2015.08.056.
[16] C. Heij, D. Dixon, P. Hadley, J. Mooij, Negative differential resistance due to single-electron switching, Appl. Phys. Lett. 74 (7) (1999) 1042–1044, https://doi.org/10.1063/1.123449.
[17] M. Hosoda, N. Ohtani, K. Tominaga, H. Mimura, T. Watanabe, Anomalously large negative differential resistance due to Γ-X resonances in type-I GaAs/AlAs superlattices, Phys. Rev. B 56 (11) (1997) 6432.
[18] C.-L. Ho, M.-C. Wu, W.-J. Ho, J.-W. Liaw, Light-induced negative differential resistance in planar inp/ingaas/inp double-heterojunction pin photodiode, Appl. Phys. Lett. 74 (26) (1999) 4008–4010, https://doi.org/10.1063/1.123243.
[19] O. Yilmazoglu, J.-P. Biethan, A. Evtukh, M. Semenenko, D. Pavlidis, H. Hartnagel, V. Litovchenko, Field emission from ZnO whiskers under intervalley electron redistribution, Appl. Surf. Sci. 258 (11) (2012) 4990–4993, https://doi.org/10.1016/j.apsusc.2012.01.153.
[20] M.K. Husain, X.V. Li, C.H. de Groot, Observation of negative differential conductance in a reverse-biased Ni/Ge Schottky diode, IEEE Electron Device Lett. 30 (9) (2009) 966–968, https://doi.org/10.1109/LED.2009.2025673.
[21] Z. Ma, F. Ren, X. Ming, Y. Long, A.A. Volinsky, Cu-doped ZnO electronic structure and optical properties studied by first-principles calculations and experiments, Materials 12 (1) (2019) 196, https://doi.org/10.3390/ma12010196.
[22] B.U. Haq, R. Ahmed, A. Afaq, A. Shaari, M. Zarshenas, Structural and electronic properties of ni-doped ZnO in zinc-blende phase: a DFT investigations, in: AIP Conference Proceedings, vol. 1482, 2012, pp. 54–57.
[23] B. Ridley, T. Watkins, The possibility of negative resistance effects in semiconductors, Proc. Phys. Soc. (1958-1967) 78 (2) (1961) 293, https://doi.org/10.1088/0370-1328/78/2/315.

[24] S. Cheung, N. Cheung, Extraction of Schottky diode parameters from forward current-voltage characteristics, Appl. Phys. Lett. 49 (2) (1986) 85–87, https://doi.org/10.1063/1.97359.

[25] R. Ocaya, F. Yakuphanoğlu, Ocaya–Yakuphanoğlu method for series resistance extraction and compensation of Schottky diode I–V characteristics, Measurement 186 (2021) 110105, https://doi.org/10.1016/j.measurement.2021.110105.

[26] S. Al-Ariki, N.A. Yahya, S.A. Al-A'nsi, M. Jumali, A. Jannah, R. Abd-Shukor, Synthesis and comparative study on the structural and optical properties of ZnO doped with Ni and Ag nanopowders fabricated by sol gel technique, Sci. Rep. 11 (1) (2021) 1–11, https://doi.org/10.1038/s41598-021-91439-1.

[27] Fytronix, IV/CV/GV characterization system, https://fytronix.com. (Accessed 4 September 2022).

[28] R. Ocaya, F. Yakuphanoğlu, A method of determining the parameters in systems with serialized Current-Voltage characteristics, J. Phys. Conf. Ser. (2021) 012077, https://doi.org/10.1088/1742-6596/2090/1/012077.

[29] I. Erol, Z. Gürler, A new methacrylate polymer functionalized with fluoroarylketone prepared by hydrothermal method and its nanocomposites with SiO_2: thermal, dielectric, and biocidal properties, Polym. Bull. (2022) 1–24, https://doi.org/10.1007/s00289-022-04195-1.

[30] E. Rhoderick, R. Williams, Metal-Semiconductor Contacts, 1988.

[31] S.M. Sze, Y. Li, K.K. Ng, Physics of Semiconductor Devices, John Wiley & Sons, NJ, United States, 2021.

[32] W. Mtangi, F.D. Auret, C. Nyamhere, P.J. van Rensburg, A. Chawanda, M. Diale, J.M. Nel, W.E. Meyer, The dependence of barrier height on temperature for Pd Schottky contacts on ZnO, Physica B, Condens. Matter 404 (22) (2009) 4402–4405, https://doi.org/10.1016/j.physb.2009.09.022.

[33] V.L. Devi, I. Jyothi, V.R. Reddy, Analysis of temperature-dependent Schottky barrier parameters of Cu–Au Schottky contacts to n-InP, Can. J. Phys. 90 (1) (2012) 73–81, https://doi.org/10.1139/p11-142.

[34] B. Gunduz, A.A. Al-Ghamdi, A. Hendi, Z.H. Gafer, S. El-Gazzar, F. El-Tantawy, F. Yakuphanoğlu, New Schottky diode based entirely on nickel aluminate spinel/p-silicon using the sol–gel spin coating approach, Superlattices Microstruct. 64 (2013) 167–177, https://doi.org/10.1016/j.spmi.2013.09.022.

[35] A.N. Donald, Semi-Conductor Physics & Devices, Tata McGraw, New Delhi, India, 2006.

[36] Y.S. Ocak, Electrical characterization of DC sputtered ZnO/p-Si heterojunction, J. Alloys Compd. 513 (2012) 130–134, https://doi.org/10.1016/j.jallcom.2011.10.005.

[37] M. Benhaliliba, A rectifying Al/ZnO/pSi/Al heterojunction as a photodiode, Micro Nanostruct. 163 (2022) 107140, https://doi.org/10.1016/j.spmi.2021.107140.

[38] M. Benhaliliba, Y. Ocak, H. Mokhtari, T. Kiliçoglu, AC impedance analysis of the Al/ZnO/p-Si/Al Schottky diode: CV plots and extraction of parameters, J. Nano-Electron. Phys. 7 (2) (2015) 02001.

[39] F. Chaabouni, M. Abaab, B. Rezig, Characterization of n-ZnO/p-Si films grown by magnetron sputtering, Superlattices Microstruct. 39 (1–4) (2006) 171–178, https://doi.org/10.1016/j.spmi.2005.08.070.

[40] S.M. Faraz, W. Shah, N.U.H. Alvi, O. Nur, Q.U. Wahab, Electrical characterization of Si/ZnO nanorod PN heterojunction diode, Adv. Condens. Matter Phys. 2020 (2020), https://doi.org/10.1155/2020/6410573.

[41] E. Nicollian, A. Goetzberger, The Si-SiO, interface–electrical properties as determined by the metal-insulator-silicon conductance technique, Bell Syst. Tech. J. 46 (6) (1967) 1055–1133, https://doi.org/10.1002/J.1538-7305.1967.TB01727.X.

[42] E.H. Nicollian, J.R. Brews, MOS (Metal Oxide Semiconductor) Physics and Technology, John Wiley & Sons, NJ, United States, 2002.

[43] A. Turut, H. Doğan, N. Yıldırım, The interface state density characterization by temperature-dependent capacitance–conductance–frequency measurements in Au/Ni/n-GaN structures, Mater. Res. Express 2 (9) (2015) 096304, https://doi.org/10.1088/2053-1591/2/9/096304.

[44] A. Rose, Concepts in Photoconductivity and Allied Problems, Interscience, NJ, United States, 1963.

[45] F. Yakuphanoglu, Photovoltaic properties of the organic–inorganic photodiode based on polymer and fullerene blend for optical sensors, Sens. Actuators A, Phys. 141 (2) (2008) 383–389, https://doi.org/10.1016/j.sna.2007.10.023.

[46] R.H. Bube, et al., Photoconductivity of Solids, RE Krieger, Florida, United States, 1978.

[47] F. Stöckmann, Photodetectors, their performance and their limitations, Appl. Phys. 7 (1) (1975) 1–5.

[48] S.A. Pehlivanoğlu, Fabrication of p-Si/n-NiO: Zn photodiodes and current/capacitance-voltage characterizations, Physica B, Condens. Matter 603 (2021) 412482, https://doi.org/10.1016/j.physb.2020.412482.

[49] M. Kumar, K.S. Gour, V.N. Singh, Photodetector performance limitations: recombination or trapping—power exponent variation with the applied bias to rescue, J. Mater. Res. 38 (2023) 1813–1823, https://doi.org/10.1557/s43578-022-00890-x.

[50] R. Ocaya, A. Dere, A.G. Al-Sehemi, A.A. Al-Ghamdi, M. Soylu, F. Yakuphanoglu, Analysis of photoconductive mechanisms of organic-on-inorganic photodiodes, Physica E, Low-Dimens. Syst. Nanostruct. 93 (2017) 284–290, https://doi.org/10.1016/j.physe.2017.06.024.

[51] M. Benhaliliba, The photovoltaic properties of a good rectifying Al/n-ZnO/p-Si/Al Schottky diode used in solar cell, J. Fund. Appl. Sci. 9 (1) (2017) 605–617, https://doi.org/10.4314/jfas.v9i1.35.

[52] M. Soylu, R. Ocaya, H. Tuncer, A.A. Al-Ghamdi, A. Dere, D.C. Sari, F. Yakuphanoglu, Analysis of photovoltaic behavior of Si-based junctions containing novel graphene oxide/nickel (II) phthalocyanine composite films, Microelectron. Eng. 154 (2016) 53–61, https://doi.org/10.1016/j.mee.2016.01.022.

[53] N. Sengouga, R. Boumaraf, R.H. Mari, A. Meftah, D. Jameel, N. Al Saqri, M. Azziz, D. Taylor, M. Henini, Modeling the effect of deep traps on the capacitance–voltage characteristics of p-type Si-doped GaAs Schottky diodes grown on high index GaAs substrates, Mater. Sci. Semicond. Process. 36 (2015) 156–161, https://doi.org/10.1016/j.mssp.2015.03.043.

[54] C.-H. Lin, C.W. Liu, Metal-insulator-semiconductor photodetectors, Sensors 10 (10) (2010) 8797–8826, https://doi.org/10.3390/s101008797.